Biomechanical study of plate and screw fixation at extra-articular fracture of the proximal radius

Nattapon Chantarapanich[1*] and Kriskrai Sitthiseripratip[2]

[1] *Department of Mechanical Engineering, Faculty of Engineering,*
Kasetsart University, Sriracha Campus, Si Racha, Chon Buri, 20230 Thailand

[2] *National Metal and Materials Technology Center,*
Khlong Luang, Pathum Thani, 12120 Thailand

Abstract

This study investigated the influence of proximal radius fracture pattern on the biomechanical performance of locking compression plate (LCP) using the finite element method. Two transverse neck fracture levels and one oblique proximal radius fracture, stabilized with stainless steel and titanium implants, were included in this study. The models of proximal radius and LCP implant set were created and virtually aligned using CAD. Four-node tetrahedral elements were used in the FE model. Articular contact pressures at the 0º, 45º, and 90º flexion angle of humeroradial ulna joint were applied to articular surface of the proximal radius. High stress concentrations were found between the proximal screws holes and around the combined holes of LCP. Elastic strain at fracture gap stabilized with implant did not significantly differ between stainless steel and titanium implants. The stainless steel implant may present higher stresses than the titanium implant, especially with a fracture close to the articular surface.

1. Introduction

Proximal radius fracture is a common fracture in the upper extremity, contributing approximately 33 percent of elbow fractures (Matsunaga *et al.*, 2009). A common mechanism leading to the fractures is an impact on the outstretched hand with an axial load on radius (El Kadi *et al.*, 2017; Matsunaga *et al.*, 2009). Plate and screw fixation is a common technique to stabilize the fracture with good success rates (Sánchez Gómez, Lajara Marco, Ricón Recarey, & Lozano Requena, 2010; Zwingmann *et al.*, 2013). However, some remaining clinical complications related to plate and screw fixation have been reported. A common complication is implant failure (Patterson *et al.*, 2001; Ring, 2008). Failure of the implant fixation requires revision surgery. In order to reduce fixation failure rates, understanding the biomechanics of plate and screw in various fracture pattern stabilizations is necessary. Many types of plate and screw fixation are available for a proximal radius fracture (Giffin, King, Patterson, & Johnson, 2004). However, the most common type is locking compression plate (LCP) (Synthes GmbH, 2016; Biomet Orthopedics, 2012; Acumed, 2017). Although the previous studies of Gutowski, Darvish, Ilyas, and Jones (2015) and Giffin *et al.* (2004) performed mechanical testing of various implant fixations for proximal radius fracture, pursuing informed implant selection, nevertheless, there is no prior report on the influences of fracture pattern, implant material, and elbow flexion, on the implant performance. These factors should significantly affect the implant selection.

*Corresponding author
  Email address: nattapon@eng.src.ku.ac.th

This study used the finite element (FE) method to assess the biomechanical performance of LCP and its screw set in various fixation conditions. Results from the analysis may greatly contribute to implant selection in managing proximal radius fractures.

2. Materials and Methods

2.1 Finite element model

A proximal radius was scanned using a Computed Tomography (CT) scanner and the data were recorded in the Digital Imaging and Communications in Medicine (DICOM) file format. These data were used to construct 3D CAD models of the proximal radius by reverse engineering. Intramedually canal and cancellous bone layers were created using CAD functions. The geometry of LCP for proximal radius fracture used in this study was approximated from the shape contour of 2-hole plate of DepuySynthes LCP Proximal radius fracture 2.4 mm (Synthes GmbH, 2016). Screws used with the LCP for proximal radius fracture are 2.4 mm diameter locking screws, and a 2.7 mm diameter cortex compression screw. The 3D model of LCP for proximal radius fracture and screw sets was created using CAD software. The fractures in this study included two levels of transverse neck fractures (10 and 15-mm distalward from articular surface) and one oblique neck fracture. Fracture gap in all cases was 1 mm. A LCP for proximal radius fracture and screw set were attached to the bone model within a Hotchkiss safe zone (Smith & Hotchkiss, 1996), as shown in Figure 1. The FE study was performed for two stages, namely the early stage of fracture healing and the stage after fracture healing.

FE models for bone and implant models were built up from four-node tetrahedral elements generated by an automatic mesh generation algorithm. Finer mesh sizes were assigned around the screw holes, LCP, and screws. The optimal element size used in all FE analyses was determined from element convergence tests.
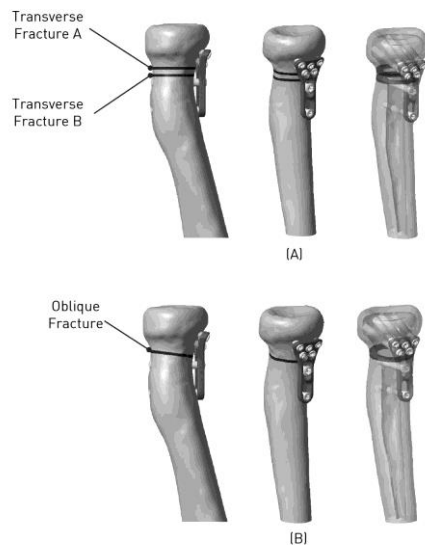

Figure 1.   3D CAD Model of (A) Transverse fracture locations, and (B) Oblique fracture location

2.2 Material properties

Table 1 shows the material properties assigned to the FE models. The material properties of cortical bone were transversely isotropic and linearly elastic, whereas the cancellous bone and implants were isotropic, homogeneous, and linearly elastic. Fracture site was assigned the properties of initial connective tissue in the early stage of fracture healing. In the stage after fracture healing, the fracture site was assigned cortical bone properties.

Table 1.   Material Properties

Materials	Elastic Modulus (MPa)	Shear Modulus (MPa)	Poisson's Ratio
Cortical Bone (Kim, Baratz, & Miller, 2017)	$E_x = E_y = 7,000$ $E_z = 11,500$	$G_{xy} = 2,600$ $G_{yz} = G_{xz} = 3,500$	$\upsilon_{xy} = \upsilon_{yz} = \upsilon_{xz} = 0.40$
Cancellous Bone (Burkhart, Quenneville, Dunning, & Andrews, 2014)	1,800	-	0.30
Initial Connective Tissue (Wei, Sun, Jao, Yeh, & Cheng, 2015)	3	-	0.40
Implant (Stainless Steel) (Chantarapanich *et al.*, 2016)	200,000	-	0.30
Implant (Titanium) (Chantarapanich *et al.*, 2016)	110,000	-	0.33

2.3 Loading conditions

Uniform contact pressure was applied to articular surface of the proximal radius. Values of applied contact pressure depend on the flexion angle of humeroradial ulna joint. 0°, 45°, and 90° flexion correspond to 1.66, 1.39, and 1.00 MPa, respectively (Cohn, Glait, Sapienza, & Kwon, 2014). Since the contact area on the articular surface of proximal radius used in this study is 101 mm², the loads matching these pressures are 168 N, 141 N, and 101 N for flexion angles of 0°, 45°, and 90°. In addition, the distal end of radial shaft was fully constrained, as shown in Figure 2.

Friction coefficients at contacts of stainless steel LCP/stainless steel screw, stainless steel LCP/bone, titanium LCP/titanium screw, and titanium LCP/bone were set at 0.15, 0.23, 0.30, and 0.36, respectively (Chantarapanich, Sitthiseripratip, Mahaisavariya, & Siribodhi, 2016). Contacts between screws and bone were constrained to no relative displacement to simulate screw purchasing. Regions where locking screw was purchased within plate hole were also constrained to no relative displacement.

2.4 Element convergence test

Four different numbers of elements were tested under loading conditions of 0° flexion with titanium implant stabilization. This convergence test is summarized in Table 2.

Figure 2.   FE Model

Table 2.   Numbers of elements and nodes in FE convergence testing

Model	Number of Elements	Number of Nodes
No.1	251,181	62,068
No.2	277,999	68,361
No.3	313,782	76,509
No.4	381,888	91,691

Magnitude of equivalent von misses (EQV) stress was used as the monitored parameter. The least number of elements that insignificantly changed the magnitude of EQV stress on the implant from that with next larger number of elements was used in FE analyses.

3. Results

3.1 Element convergence

In all cases, the maximum EQV stress occurred around the contact of distal screw and combined hole of LCP. Figure 3 shows the element convergence test results. It can be seen that maximum EQV stress values in the convergence testing models No.2, No.3, and No.4 were within 6.8 percent. As a result, the optimal model for FE analysis was model No. 2 with finite element count 277,999 and 68,361 nodes.

3.2 Stress distribution

Maximum EQV stress on the implant was found at the contact between compression screw and LCP. A stress concentration region was located between the proximal screw holes and around the combined holes of LCP. In the early stage of fracture healing, EQV stress reached its maximum in all fracture cases at 0° flexion angle. In most cases, fracture level A showed higher EQV stress than fracture level B or oblique fracture. The stainless steel implant had higher EQV levels than the titanium implant: the EQV stress level was 343.3–611.6 MPa for the stainless steel implant and 210.1–332.8 MPa for the titanium implant. In the stage after fracture healing, EQV stresses were of lower magnitude. Figure 4, Figure 5 and Table 3 show the EQV stresses on implant and bone for the different fracture patterns and the implant materials.

High bone stress presented around the compression screws holes on the outer side of cortical bone. It reached its maximum at 0° flexion angle and decreased with the flexion angle. However, the differences in bone stress with all flexion angles as well as in the implant materials were not significant. In addition, there was also no significant difference in bone stress between the transverse fracture A and the transverse
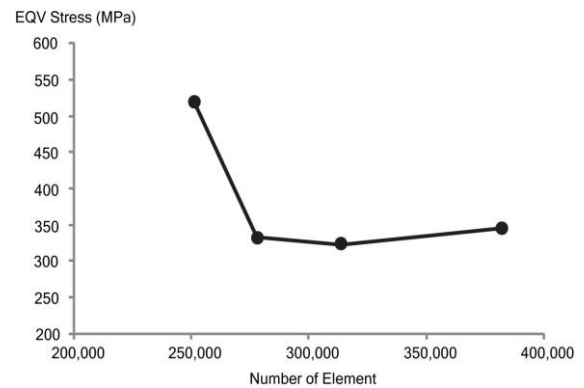

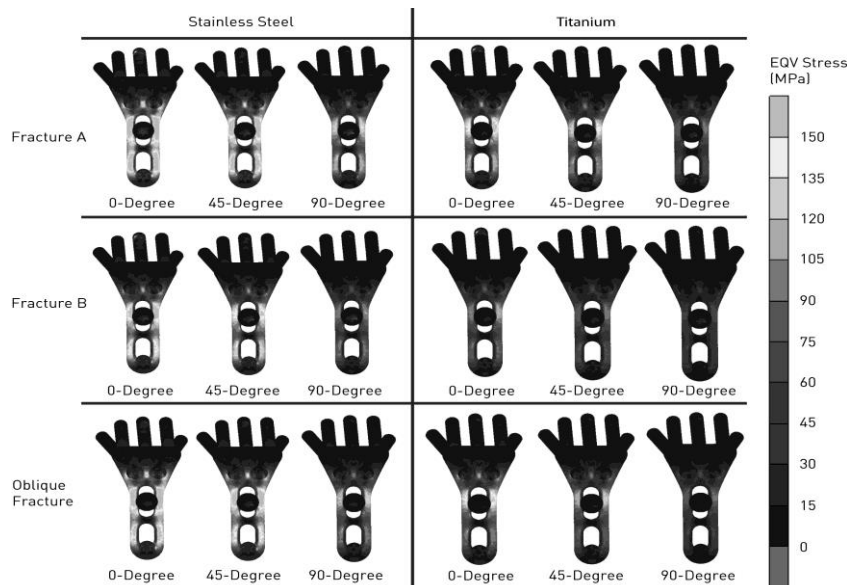Figure 3.   Convergence testing result

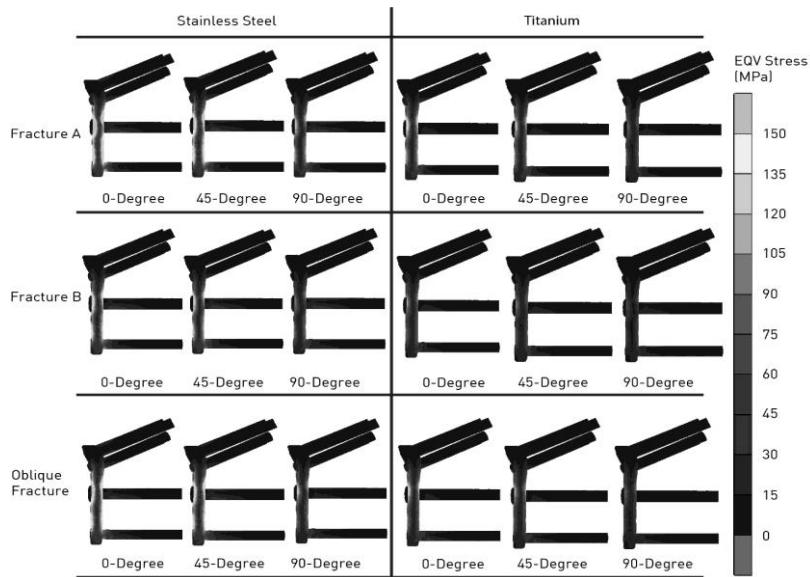Figure. 4.   Implant EQV stress (Front view of implant)

Figure 5.   Implant EQV stress (Side view of implant)

Table 3.   Implant EQV stress (MPa)

Fracture Type	Flexion Angle	Stage of Early Fracture Fixation		Stage of After Fracture healing	
		Stainless Steel	Titanium	Stainless Steel	Titanium
Transverse Level A	0°	611.6	332.8	272.4	254.3
	45°	459.5	301.0	213.4	115.6
	90°	377.4	218.6	212.6	176.6
Transverse Level B	0°	429.0	315.8	272.4	254.3
	45°	389.3	243.6	213.4	115.6
	90°	373.2	221.4	212.6	176.6
Oblique	0°	542.6	331.2	272.4	254.3
	45°	493.0	286.4	213.4	115.6
	90°	343.4	210.1	212.6	176.6

fracture B. Nevertheless, for the oblique fracture case, the stress was highest among the cases simulated. Average value of the bone stress in the early stage of fracture healing ranged within 28.9–56.4 MPa for the stainless steel and in 30.2–64.2 MPa for the titanium. In the stage after fracture healing, bone stress had a lower magnitude. Table 4 shows the bone stress for different fracture patterns and implant materials.

3.3 Fracture displacement and stability

The displacement of fracture tends to move medial-ward (opposite to LCP), when viewed in a neural position. Elastic strain in the fracture gap for fracture level A was the largest among the fracture types under consideration. In all fracture cases, elastic strain reached its maximum at 0° flexion angle. A large difference was observed between elastic strains in the early stage of fracture healing and in the stage after fracture healing. Table 5 shows the elastic strains at the fracture gap.

4. Discussion

The FE method allows assessing the biomechanical performance of an LCP plate and screws used to stabilize the proximal radius fracture, as well as stresses in the bone. The

material models assigned in this study were transverse isotropic models, which give reliable results in a study of biomechanics of proximal radius bone.

The FE results had maximum EQV stress between proximal screw holes and around the combined holes of LCP. This is because the load diverts from the fracture region, which has a low elastic modulus, by transfer to the LCP structure via screw contact. The maximum EQV stress exhibited in this region corresponds well to the clinical observations, according to which the implants usually break around this region (Patterson et al., 2001; Ring, 2008). Lateral side of the fracture site is stabilized with LCP whereas no implant is buttressed on the medial side of the fracture site. Due to the physiological loads applied on the articular surface of proximal radius, proximal part of the fracture moves easily on medial side. The LCP is then subsequently subject to a bending load, increasing the magnitude of EQV stress on the bending point.

EQV stress on the implant decreases with the elbow flexion angle. At neutral position of elbow (0° flexion) it has its maximum value. This finding encourages to make the patients aware not to extend the elbow joint fully straight, and to avoid some daily activities such as pushing the table floor.

EQV stresses in the stainless steel implants were higher than in the titanium implants. The use of titanium implant can therefore reduce the chances of implant failure.

Table 4.   Bone stress (MPa)

Fracture Type	Flexion Angle	Stage of Early Fracture Fixation		Stage of After Fracture healing	
		Stainless Steel	Titanium	Stainless Steel	Titanium
Transverse Level A	0º	37.7	40.3	25.4	13.0
	45º	33.4	38.0	18.0	13.6
	90º	28.9	30.6	18.7	21.5
Transverse Level B	0º	35.8	40.0	25.4	13.0
	45º	33.9	36.0	18.0	13.6
	90º	29.2	30.2	18.7	21.5
Oblique	0º	56.4	64.2	25.4	13.0
	45º	50.1	53.4	18.0	13.6
	90º	33.5	38.2	18.7	21.5

Table 5.   Elastic strain ($\mu\varepsilon$)

Fracture Type	Flexion Angle	Stage of Early Fracture Fixation		Stage of After Fracture healing	
		Stainless Steel	Titanium	Stainless Steel	Titanium
Transverse Level A	0º	447.7	516.2	0.4	0.3
	45º	398.6	458.9	0.3	0.2
	90º	269.1	310.5	0.3	0.3
Transverse Level B	0º	219.5	244.8	0.6	0.3
	45º	194.7	204.3	0.4	0.2
	90º	130.9	146.8	0.4	0.4
Oblique	0º	359.1	406.6	0.5	0.4
	45º	319.0	338.8	0.5	0.4
	90º	212.7	242.8	0.4	0.4

However, the titanium implants have poorer fracture stability than the stainless steel implants, due to larger elastic strains. This finding correlates well with the previous studies of Chantarapanich *et al.* (2016) and Taheri, Blicblau, and Singh (2011), who found similar behavior in other orthopaedic implants.

Fracture level A close to the proximal radius articular surface tends to have larger EQV stresses than the more distalward fracture levels. At full extension, the stress on the stainless steel implant is close to the yield strength of this material, as the typical yield stress for stainless steel ranges from 750 to 960 MPa (Chantarapanich *et al.*, 2016). As a result, the titanium implant is considered a good alternative to stabilize the proximal radius fracture. For a more distal transverse fracture site, the EQV stresses on the implant are lower than with fracture level A, about 95-80 percent of stress exhibited with fracture level A at 0º and 45º flexion for titanium implant, and 70–85 percent of stress with fracture level A at 0º and 45º flexion for stainless steel implant. The EQV stress did not significantly differ between stainless steel and titanium implants at 90º elbow flexion. As a result, a stainless steel implant can be used instead of a titanium implant for more distal fracture sites.

With an oblique fracture, the EQV stress in a stainless steel implant is much higher than in a titanium implant. Thus, a good choice for stabilizing oblique fracture is the titanium implant.

Since titanium implants produce elastic strains larger than stainless steel implants, titanium implants give poorer fracture stability than stainless steel implants. This is because titanium is less stiff than stainless steel, and has larger deformations. From the results in Table 5, the elastic strain in stainless steel implants is 5-13 percent less than in titanium

implants, with greatest difference in elastic strain in the case of fracture level A. Hence, in all fracture types considered in this study, the EQV stress is the more important point to be taken into account on implant selection.

In addition, at the stage after fracture healing, EQV stresses and equivalent elastic stain are lesser in magnitude. The EQV stresses in the stage after fracture healing are below the cyclic strength of materials (350 MPa for stainless steel and 560 MPa for Titanium) (Teoh, 2000), so it is safe to retain the implant in the body. In addition, there is no difference in fracture stability after healing.

In the early stage of fracture healing and the stage after fracture healing, bone stresses are much below the yield strength of cortical bone, which is 122.3 MPa (Currey, 2004), with both stainless steel and titanium implants. There is a low chance of bone breakage during and after the healing period. Hence, bone stress insignificantly affects the implant selection in this case. This is in contrast to long bone fixation, such as of instant femur, in which bone stress influences the stability of implant during and after healing (Sitthiseripratip *et al.*, 2003).

5. Conclusions

This study used the FE method in a biomechanical study of LCP and screw set stabilizing various fractures types in the proximal radius region. Elastic strain at fracture site is higher with titanium implant than with steel implant. However, the values differ only slightly. Therefore, the first priority in considering implant selection for radial head fracture is EQV stress. In all fracture types, the most critical flexion that produces the highest EQV stresses is with 0º flexion angle. Transverse fracture close to the articular surface with 0º

flexion can lead to high EQV stress in both stainless steel and titanium implants. Especially in a stainless steel implant, the stress can reach the yield strength of this material. Titanium LCP and screw implants are preferable to stabilize a transverse fracture in the more proximal to articular surface, and oblique fracture, whereas stainless steel LCP and screw implants can be preferred alternative for transverse fracture located more distalward. Bone stress level is relatively low with both stainless steel and titanium implants during the early stage of fracture healing, and also in the stage after fracture healing, so this aspect is not important in decisions on implant selection.

References

Acumed. (2017). Radial Head Plating System Surgical Technique. Retrieved from http://www.acumed.net/system/files/Acumed-Surgical-Technique-EN-Locking-Radial-Head-Plates-ELB00-02-B-new.pdf

Biomet Orthopedics. (2012). A. L. P. S. Elbow Plating System. Retrieved from http://www.zimmerbiomet.com/content/dam/zimmer-biomet/medical-professionals/trauma/alps-elbow-fracture-system/alps-elbow-system-sales-sheet.pdf

Burkhart, T. A., Quenneville, C. E., Dunning, C. E., & Andrews, D. M. (2014). Development and validation of a distal radius finite element model to simulate impact loading indicative of a forward fall. *Proceedings of the Institution of Mechanical Engineers, Part H: Journal of Engineering in Medicine 228*(3), 258–271. doi:10.1177/0954411914522781

Chantarapanich, N., Sitthiseripratip, K., Mahaisavariya, B., & Siribodhi, P. (2016). Biomechanical performance of retrograde nail for supracondylar fractures stabilization. *Medical and Biological Engineering and Computing, 54*(6), 939–952. doi:10.1007/s11517-016-1466-0

Cohn, M., Glait, S. A., Sapienza, A., & Kwon, Y. W. (2014). Radiocapitellar joint contact pressures following radial head arthroplasty. *Journal of Hand Surgery, 39*(8), 1566–1571. doi:10.1016/j.jhsa.2014.05.021

Currey, J. D. (2004). Tensile yield in compact bone is determined by strain, post-yield behaviour by mineral content. *Journal of Biomechanics, 37*(4), 549–556. doi:10.1016/j.jbiomech.2003.08.008

El Kadi, K., Benabid, M., Saliou, S., El Assil, O., Marzouki, A., Lahrach, K., & Boutayeb, F. (2017). Simultaneous ipsilateral fractures of distal and proximal ends of the radius. *Pan African Medical Journal, 27*, 98. doi:10.11604/pamj.2017.27.98.3504

Giffin, J. R., King, G. J. W., Patterson, S. D., & Johnson, J. A. (2004). Internal fixation of radial neck fractures: An in vitro biomechanical analysis. *Clinical Biomechanics, 19*(4), 358–361. doi:10.1016/j.clinbiomech.2004.01.003

Gutowski, C. J., Darvish, K., Ilyas, A. M., & Jones, C. M. (2015). Comparison of crossed screw versus plate fixation for radial neck fractures. *Clinical Biomechanics, 30*(9), 966–970. doi:10.1016/j.clinbiomech.2015.07.001

Kim, S., Baratz, M. E., & Miller, M. C. (2011). Contact Stress Analysis of the Elbow Joint; Design of Radial Head Replacements. *Transactions of the Orthopaedic Research Society Annual Meeting, 36*, 567. Retrieved from https://www.ors.org/Transactions/57/0567.pdf

Matsunaga, F. T., Tamaoki, M. J. S., Cordeiro, E. F., Uehara, A., Ikawa, M. H., Matsumoto, M. H., . . . Belloti, J. C. (2009). Are classifications of proximal radius fractures reproducible? *BMC Musculoskeletal Disorders, 10*, 120. doi:10.1186/1471-2474-10–120

Patterson, J. D., Jones, C. K., Glisson, R. R., Caputo, A. E., Goetz, T. J., & Goldner, R. D. (2001). Stiffness of simulated radial neck fractures fixed with 4 different devices. *Journal of Shoulder and Elbow Surgery, 10*(1), 57–61. doi:10.1067/mse.2001.109558.

Ring, D. (2008). Displaced, unstable fractures of the radial head: Fixation vs. replacement-What is the evidence? *Injury, 39*(12), 1329–1337. doi:10.1016/j.injury.2008.04.011

Sánchez Gómez, P., Lajara Marco, F., Ricón Recarey, F. J., & Lozano Requena, J. A. (2010). Radial head comminuted fractures: A comparative study between resection and internal fixation. *Revista Espanola de Cirugia Ortopedica y Traumatologia, 54*(5), 280–288. doi:10.1016/S1988-8856(10)70247-9

Sitthiseripratip, K., Van Oosterwyck, H., Vander Sloten, J., Mahaisavariya, B., Bohez, E. L. J., Suwanprateeb, J., . . . Oris, P. (2003). Finite element study of trochanteric gamma nail for trochanteric fracture. *Medical Engineering and Physics, 25*(2), 99–106. doi:10.1016/S1350-4533(02)00185-6

Smith, G. R., & Hotchkiss, R. N. (1996). Radial head and neck fractures: anatomic guidelines for proper placement of internal fixation. *Journal of Shoulder and Elbow Surgery, 5*(2), 113–117. doi:10.1016/S1058-2746(96)80005-X

Synthes GmbH. (2016). LCP Proximal Radius Plates 2.4 Surgical Technique. Retrieved from https://emea.depuysynthes.com/json?amid=MEDIA_BIN_AJAX&mbid=036.000.681

Taheri, N. S., Blicblau, A. S., & Singh, M. (2011). Comparative study of two materials for dynamic hip screw during fall and gait loading: titanium alloy and stainless steel. *Journal of Orthopaedic Science, 16*(6), 805–813. doi:10.1007/s00776-011-0145-0

Teoh, S. H. (2000). Fatigue of biomaterials: A review. *International Journal of Fatigue, 22*(10), 825-837. doi:10.1016/S0142-1123(00)00052-9

Wei, H. W., Sun, S. S., Jao, S. H., Yeh, C. R., & Cheng, C. K. (2005). The influence of mechanical properties of subchondral plate, femoral head and neck on dynamic stress distribution of the articular cartilage. *Medical Engineering and Physics, 27*(4), 295–304. doi:10.1016/j.medengphy.2004.12.008

Zwingmann, J., Welzel, M., Dovi-Akue, D., Schmal, H., Südkamp, N. P., & Strohm, P. C. (2013). Clinical results after different operative treatment methods of radial head and neck fractures: A systematic review and meta-analysis of clinical outcome. *Injury, 44*, 1540–1550. doi:10.1016/j.injury.2013.04.003